Received: 9 February 2024 | Revised: 8 April 2024 | Accepted: 9 April 2024

DOI: 10.1111/ter.12717

RESEARCH ARTICLE

Terra Nova WILEY

U-Pb carbonate dating reveals long-lived activity of proximal margin extensional faults during the Alpine Tethys rifting

M. Rocca[1] | S. Zanchetta[1] | M. Gasparrini[2] | X. Mangenot[3] | F. Berra[2] | P. Deschamps[4] | A. Guihou[4] | A. Zanchi[1]

[1]Department of Earth and Environmental Sciences, University of Milano-Bicocca, Milan, Italy

[2]Earth Sciences Department, University of Milan, Milan, Italy

[3]H-Expertise Services, Pomps, France

[4]Aix Marseille Univ, CNRS, IRD, INRAE, CEREGE, Aix-en-Provence, France

Correspondence
M. Rocca, Department of Earth and Environmental Sciences, University of Milano-Bicocca, Milan 20126, Italy.
Email: m.rocca@campus.unimib.it

Funding information
Ministero dell'Università e della Ricerca

Abstract

Syn-rift extensional faults play a significant role during the early stage of rifting. Constraining the age of faulting, and how and when deformation shifts from the proximal to the distal margin areas, is crucial for the reconstruction of the rifting process. Previous assessments of the structural and temporal evolution of rift-related faults of the Adria proximal margin have primarily relied on indirect biostratigraphic evidence. Additionally, the majority of rift-related faults underwent tectonic inversion during the Alpine orogeny. In this study, in-situ U-Pb geochronology was applied on syn-kinematic calcites to unravel the activity of the Amora Fault, a remarkable example of a Jurassic growth fault unaffected by the Alpine orogeny. The obtained ages, spanning from Hettangian to Callovian, extend the AF activity beyond the previously established Early Jurassic time. This chrono-structural model has significant implications on the role of major extensional faults in focusing deformation throughout the rift system's evolution.

KEYWORDS
Alpine Tethys, extensional faults, Jurassic rifting, Southern Alps, U-Pb carbonate dating

1 | INTRODUCTION

The rifting of the Alpine Tethys began in the Early Jurassic (Late Hettangian) because of the propagation of the Central Atlantic rifting, which marks the onset of Pangea break-up (Chenin et al., 2022; Frizon De Lamotte et al., 2015; Manatschal et al., 2022; Manatschal & Bernoulli, 1998; Winterer & Bosellini, 1981). This major stretching event affected the central Southern Alps (cSA; Figure 1a), which became the proximal domain of the Southern Adria margin. This latter was characterized by deep basins and structural highs and bounded by N-S trending extensional faults forming the Lombardian Basin (Bernoulli, 1964; Bertotti et al., 1993; Figure 1b). The main faults were characterized by listric geometries rooting at middle-upper crustal depths (Bertotti et al., 1993; Berra & Carminati, 2009; Figure 1b).

Temporal and structural evolution of fault systems of the Lombardian Basin has long been inferred based on field geometrical relationships recording syn-depositional tectonics revealed by drastic changes in facies and sediment thickness distribution. Recently, absolute dating of brittle structures has become possible with the advent of in-situ carbonate U-Pb geochronology via LA-ICPMS (Bilau et al., 2023; Nuriel et al., 2017, 2019; Roberts & Walker, 2016). When dating carbonate phases to reconstruct fault activity, it is fundamental to link the carbonate precipitation event to fault kinematics and to provide robust evidence that the dated material formed contemporaneously to fault activation or reactivation

(Roberts & Holdsworth, 2022). This requires a pre-dating multidisciplinary screening protocol, including structural, microstructural, petrographic and stable isotope characterization, which has all been implemented in this work.

This study aims at constraining the onset of Jurassic rifting event in the Lombardian Basin of the cSA by employing U-Pb LA-ICPMS radiometric dating of fault-related calcites. The Amora Fault (AF; Figures 1b and 2b,c) stands out as an ideal candidate, since it represents a persistent, long-living, growth fault that broadly escaped later tectonic reactivation during the Alpine compressions. Integration of structural, stratigraphic, geochemical and geochronological data shed new light on the geodynamic activity of one of the main extensional structures related to the onset of the Jurassic rifting.

2 | GEOLOGICAL SETTING

Placed south of the Periadriatic Fault, the cSA consists of a polyphase S-verging fold-and-thrust belt active at upper crustal levels since Late Cretaceous (Schönborn, 1992; Zanchetta et al., 2015; Figure 2a). The Amora Fault is part of a broader N-S trending fault system displacing the Mesozoic succession of the southern portion of cSA (Figures 1b and 2). A wealth of data (Bernoulli, 1964; Berra et al., 2009; Berra & Carminati, 2009; Bertotti et al., 1993) documents that the AF and related faults are extensional structures controlling the evolution of the Adria passive margin since the inception of crustal stretching leading to the opening of the Alpine Tethys.

The onset of extensional regimes in the cSA is recorded by tectonic collapse of Upper Triassic to Hettangian shallow sea carbonate platform facies (pre-rift succession; Jadoul & Galli, 2008; Figure 2b) due to the activation of N-S trending normal faults separating subsiding basins from structural highs (Bernoulli, 1964; Gaetani, 1975; Bertotti et al., 1993; Figures 1 and 2).

During Sinemurian–early Pliensbachian, subsidence increased rapidly in the Lombardian Basin, where lower Hettangian pre-rift successions were conformably covered by basinal facies of the Moltrasio Limestone (Sinemurian; Gaetani, 1975) up to 3 km thick (Mt. Generoso Basin; Bernoulli, 1964), which represent syn-rift sedimentation (Bertotti et al., 1993, 1999; Berra et al., 2009; Figures 1b and 2b). Then, by the end of Pliensbachian, basins reached their maximum tectonic subsidence that gradually decreased from Toarcian to Aptian times (Berra & Carminati, 2009; Santantonio & Carminati, 2011). Previous studies (Berra et al., 2009; Berra & Carminati, 2009; Bertotti et al., 1993; Incerpi et al., 2020; Manatschal et al., 2022; Santantonio & Carminati, 2011) documented that the main bordering faults were active between Hettangian and early Pliensbachian (Figure 1b); later, extension shifted westward (late Pliensbachian to Toarcian).

The AF borders a N-S trending basin (Mt. Rena half-graben; Figures 1b and 2b,c) filled by about 1 km of basinal limestones. The AF exhibits a vertical displacement of more than 600 m, juxtaposing the Moltrasio Limestone to the Zu Limestone (Figure 2b,c). Sedimentary breccias reworking older units and m-thick slumps characterize the base of Moltrasio Limestone in the AF hangingwall (Lb; Figures 2b, 3d,e). The latter shows, together with the overlying Domaro Limestone, a marked increase in thickness up to 650 m in Mt. Rena half-graben. The lowermost Jurassic succession is remarkably thinner in the AF footwall (Mt. Poieto high; Figure 2b) or totally missing (Nese high; Figure 1b; Bersezio et al., 1997; Casati & Gaetani, 1968). West of Mt. Poieto–Nese structural high, the Concesio Group is replaced by the Sogno Formation (Figure 1b; Bertotti et al., 1993, Erba et al., 2022), suggesting that the AF forms the boundary of a N-S trending structural high.

Significance Statement

The present manuscript investigates the onset of Jurassic rifting in the proximal Adria margin, employing a novel approach that integrates structural and biostratigraphic information with in-situ U-Pb dating of syn-tectonic calcite. This innovative integrated methodology highlights the long-lived nature of extensional faults active at shallow crustal levels in the Italian Southern Alps, confirming the existence of well-preserved Jurassic fault systems that escaped subsequent reactivation during the Alpine orogeny. Moreover, it represents a significant advance in understanding the long-term behaviour of extensional faults. Specifically, the application of in-situ U-Pb dating of syn-tectonic calcites provides crucial insights into the timing of fault activity. These results contribute not only to the understanding of the geological evolution of the Italian Southern Alps but also to the current knowledge regarding the application of U-Pb dating of carbonates in timing past fault activity. This work stems from several years of fieldwork in the region and has not been published previously.

3 | SAMPLES AND METHODS

Fault-related samples come from Zu Limestone, upper Norian to Rhaetian in age. The analysed samples were collected from high-angle, dip-slip N-S trending normal faults with displacements of up to a few metres from arrays of domino-style tilted blocks and Andersonian horst and graben structures, in the AF footwall (Figures 2c and 3). Samples are mainly fracture-filling carbonate cements from bed-normal syn-tectonic veins (tension gashes), as well as calcite cements filling stylolites or forming stepped slickenfibres. Geometric relationships between mesoscale faults and carbonate veins were investigated to identify rift-related syn-tectonic carbonate cements. Striated faults were also analysed in terms of palaeo-stress reconstruction by means of Win-Tensor (Delvaux &

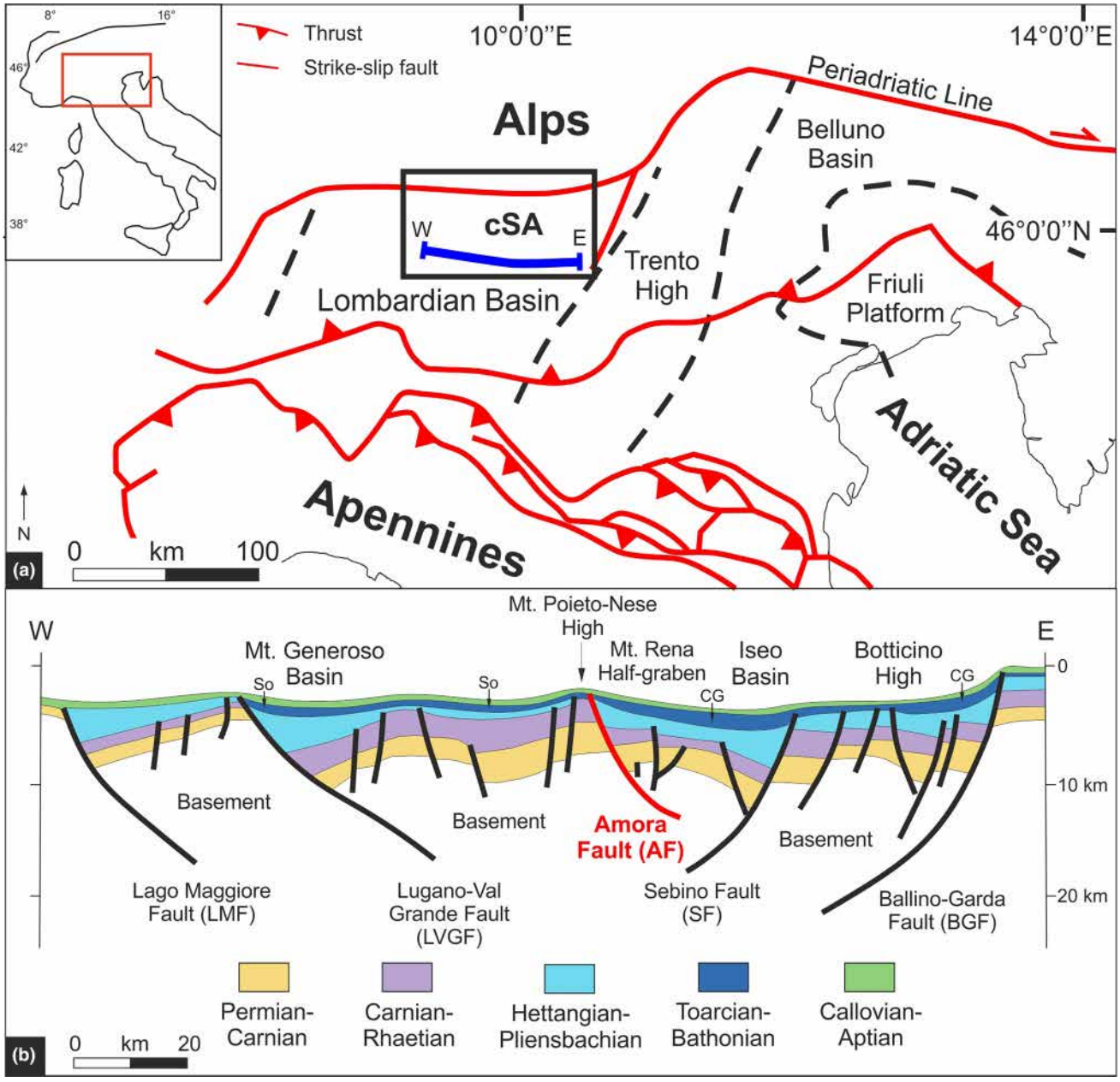

FIGURE 1 (a) Tectonic map of Northern Italy. The dashed lines define the borders between basins and highs during the Mesozoic rifting. The black rectangle includes the central Southern Alps (cSA) area, and the blue W-E transect illustrates the location of the section in B (after Berra & Carminati, 2009). (b) Architecture of the Lombardian Basin at the end of the Early Cretaceous (modified from Berra & Carminati, 2009). CG-Concesio Group and So-Sogno Formation. [Colour figure can be viewed at wileyonlinelibrary.com]

Sperner, 2003; Figure 3b,g, see also Supporting information S1). Moreover, statistical analysis of slump folds was applied following the methodology described by Naves De Lima Rodrigues et al. (2021) to strengthen the relationship between the AF and the sedimentary record (Figure 3f and Supporting information S1).

According to microstructural analyses, including optical and cathodoluminescence petrography, performed on 15 samples, all samples were investigated for the O-C stable isotope composition and 6 samples were selected for U-Pb dating (see Supporting information for details on sample localities, analytical methods and procedures).

4 | RESULTS

Petrography led to the identification of several generations of carbonate cement. To elucidate the activation and progression of AF, U-Pb analyses were exclusively conducted on the first cement, given by a non-ferroan calcite cement (Cal-1; Figure 4).

Cal-1 is composed of elongated-blocky or blocky crystals (0.5–2 mm) displaying a uniform dull red luminescence, like the one of the host-rock (Figure 4). Six samples of Cal-1 from Zu Limestone (one fault surface, two stylolites and three tension gashes) were analysed.

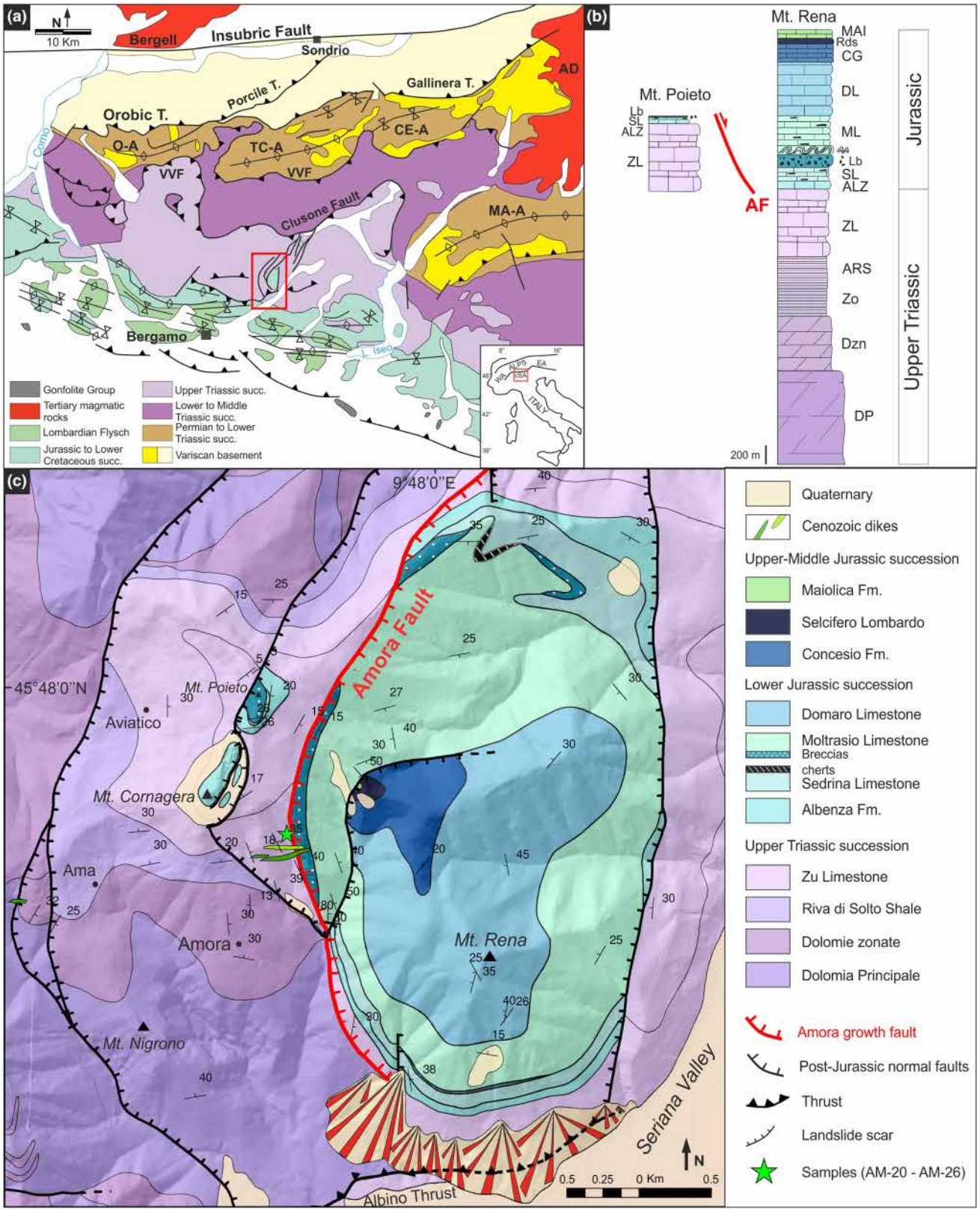

FIGURE 2 (a) Geological scheme of the cSA modified from Zanchetta et al. (2015). The red square shows the location of the study area. AD-Adamello Batholith; CE-A-Cedegolo Anticline; MA-A-Monte Alto Anticline; TC-A-Trabuchello-Cà Bianca Anticline; O-A-Orobic Anticline; and VVF-Valtorta-Valcanale Fault. (b) Stratigraphic log of the Mt. Rena and Mt. Poieto successions. AF-Amora Fault. (c) Geological map of the Seriana Valley area showing the Amora Fault and sampled locations. [Colour figure can be viewed at wileyonlinelibrary.com]

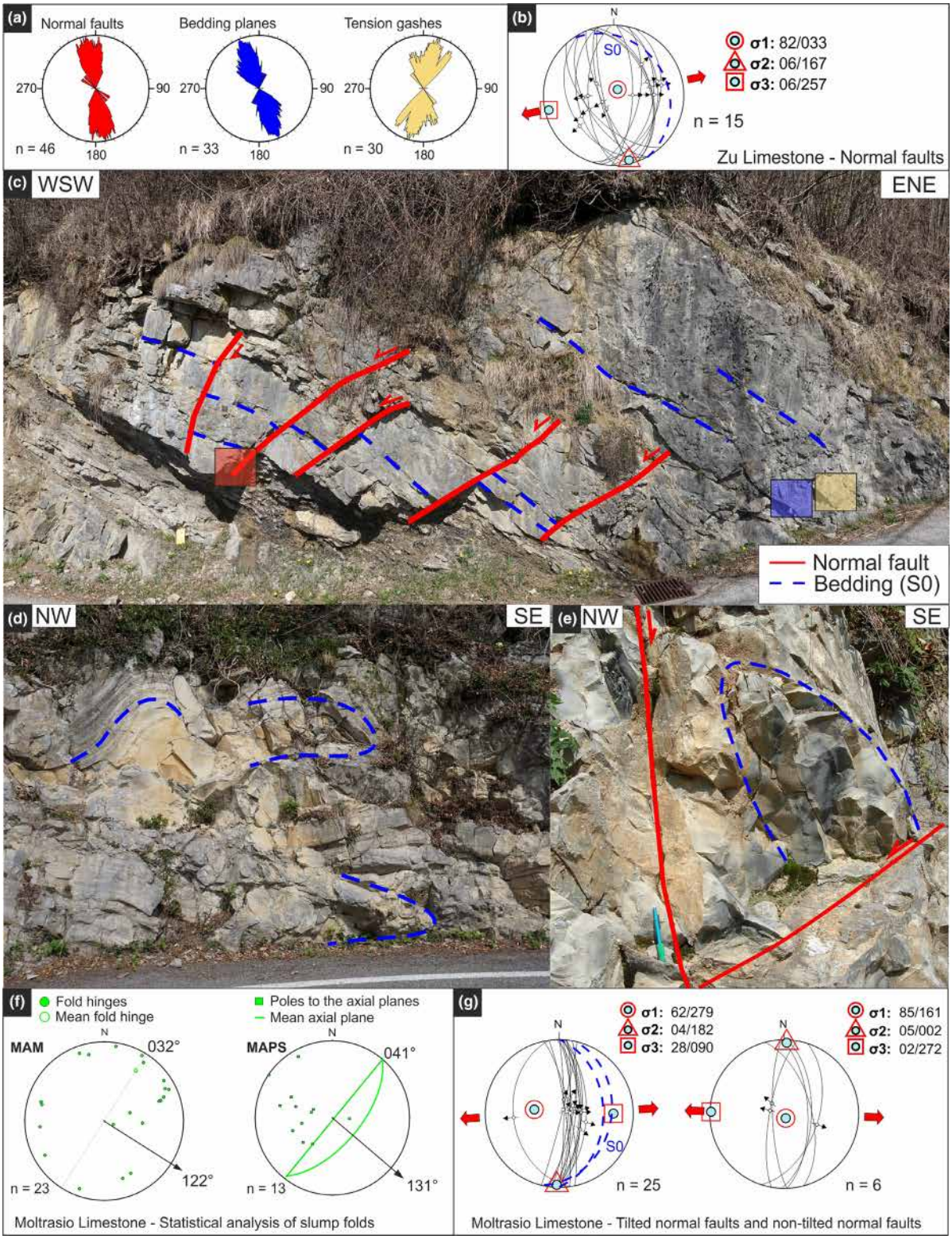

FIGURE 3 (a) Rose diagrams with the strike of faults, beds and tension gashes measured in Zu Limestone (ZL; footwall of AF) and in Moltrasio Limestone (ML; hangingwall of AF). (b) Palaeo-stress solutions from normal faults in the footwall (ZL). (c) The picture shows mesoscopic tilted blocks displaced by domino-style normal faults with Andersonian horst and graben structures. The three squares indicate the sampling sites of the structures bearing the analysed carbonate cements (red—slickenfibres on fault planes; blue—stylolites-filling calcite; and yellow—tension gashes). (d) Slump folds in the hangingwall of AF (ML). (e) Slump fold and a tilted normal fault crosscut by a non-tilted normal fault in ML. (f) Results of statistical analysis of slump folds (ML) with mean axis method (MAM; Woodcock, 1979) and mean axial plane strike method (MAPS; Alsop & Marco, 2012). The arrow indicates the transport direction of sediment along the palaeo-slope. A detailed description of the methods can be found in Supporting information S1. (g) Palaeo-stress solutions from normal faults in the hangingwall (ML). [Colour figure can be viewed at wileyonlinelibrary.com]

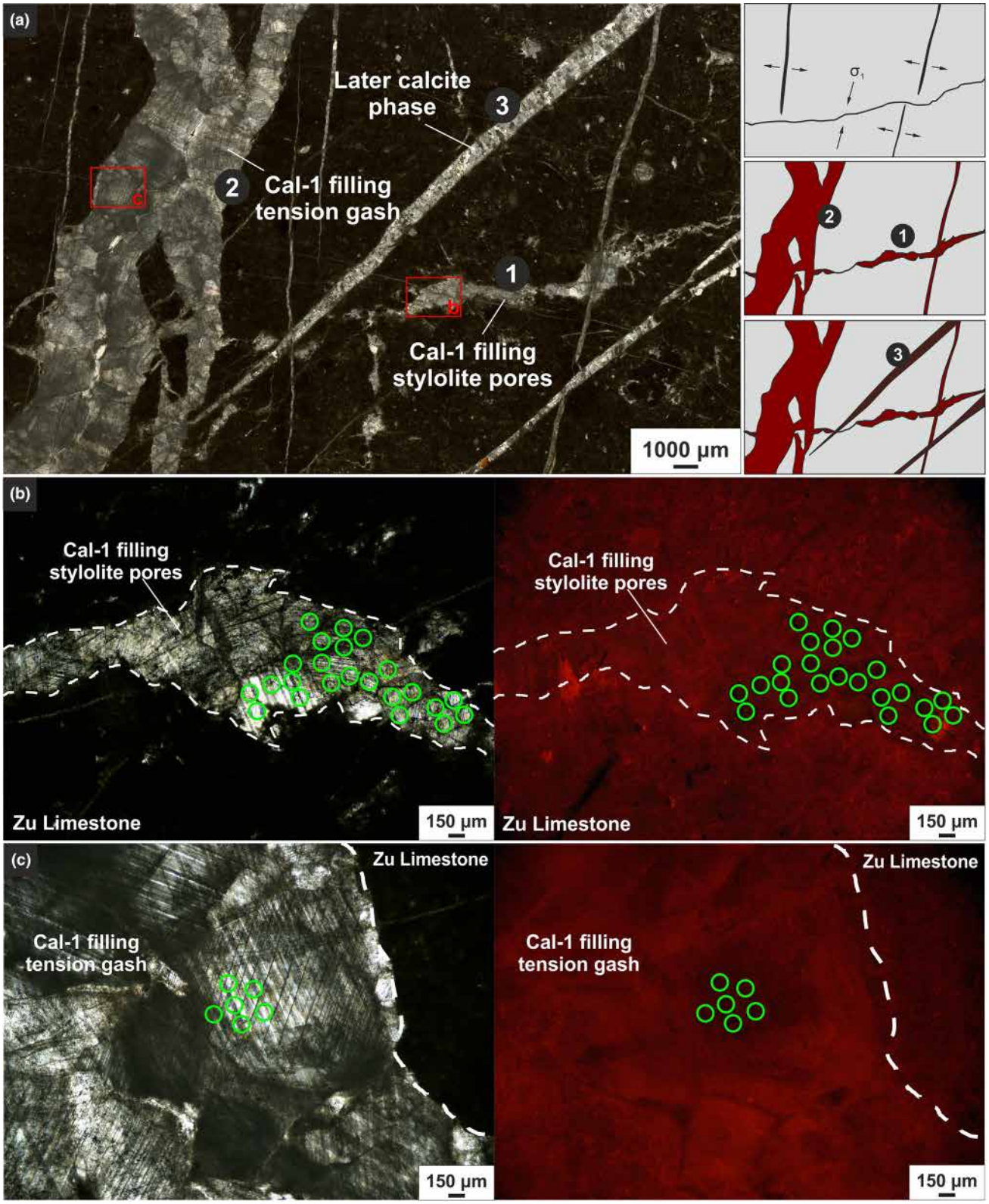

FIGURE 4 (a) Plane-polarized light image illustrating cross relationships between calcite-filled tension gashes and stylolites. The simplified sketch on the right shows the progressive formation and sealing of veins and stylolites. The red squares refer to panels b and c. (b) Zoom on dated Cal-1 in a stylolite pore. The green circles correspond to the U-Pb ablation spots. (c) Zoom on dated Cal-1 in a tension gash. The green circles correspond to the U-Pb ablation spots. [Colour figure can be viewed at wileyonlinelibrary.com]

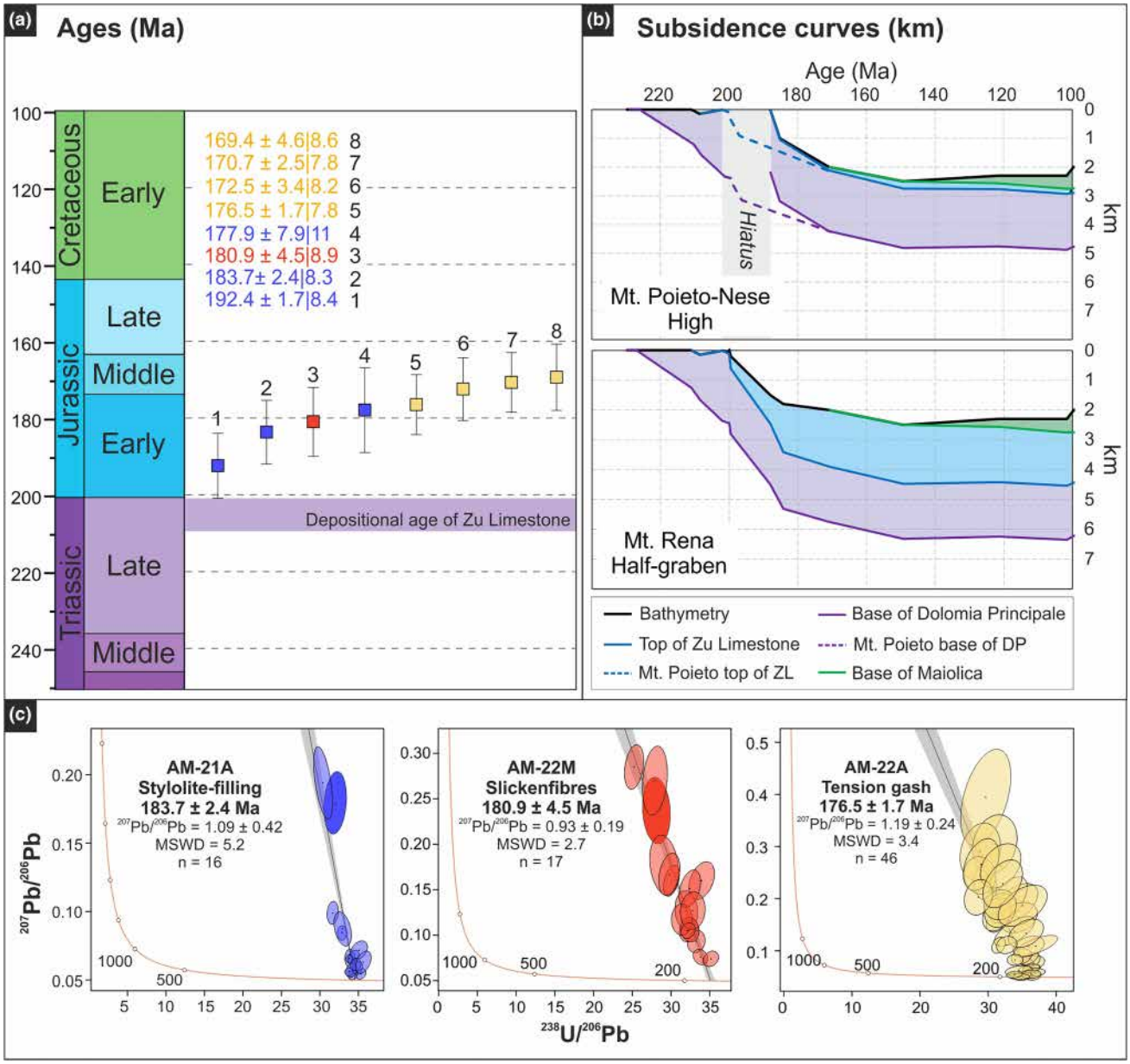

FIGURE 5 (a) Summary of obtained U-Pb ages (squares with 2σ systematic errors and colours corresponding to Figure 2c). Both 2σ internal and systematic errors are reported in the legend. (b) Calculated decompacted total subsidence curves of the Mt. Poieto–Nese high (top) and Mt. Rena half-graben (bottom) successions. The curves are calculated for the base of the Dolomia Principale (Upper Carnian–Norian), the top of the Zu Limestone and the base of the Maiolica (Tithonian–Lower Aptian). The dashed lines represent the subsidence curve of Mt. Poieto high, where the Hettangian succession is remarkably reduced, while the hiatus pertains to Nese high, where it is absent. (c) Tera–Wasserburg plots showing $^{238}U/^{206}Pb$ versus $^{207}Pb/^{206}Pb$ for three of the analysed syn-kinematic calcites (with 2σ internal errors). The colour of the ellipses corresponds to ages in (a). [Colour figure can be viewed at wileyonlinelibrary.com]

$\delta^{13}C_{carb}$ and $\delta^{18}O_{carb}$ compositions of Cal-1 range from 2.5 to 3.4 ‰ VPDB and from −4.2 to −2.6 ‰ VPDB, respectively, and are similar to those of the host-rock displaying $\delta^{13}C_{carb}$ and $\delta^{18}O_{carb}$, respectively, in the range 2.9/3.6 ‰ VPDB and −3.5/−1.5 ‰ VPDB (see Supporting information S2).

Measured U and Pb isotopic ratios display Tera–Wasserburg linear regressions (isochrons) pointing towards a common initial $^{207}Pb/^{206}Pb$ composition of 0.8656 ± 0.0062 and MSWD (mean standard weighted deviation) between 1.7 and 5.3. All Tera–Wasserburg diagrams show either a large spread in the U-Pb ratios or data close to the radiogenic end-member advocating the robustness of the calculated U-Pb ages (Figure S3). Ages range between 192.4 ± 1.7|8.4 Ma and 169.4 ± 4.6|8.6 Ma (we report both the uncertainty of the lower intercept age—2σ internal and the error propagation—2σ systematic; see Supporting information S3) and are systematically younger than the host-rock stratigraphic age (late

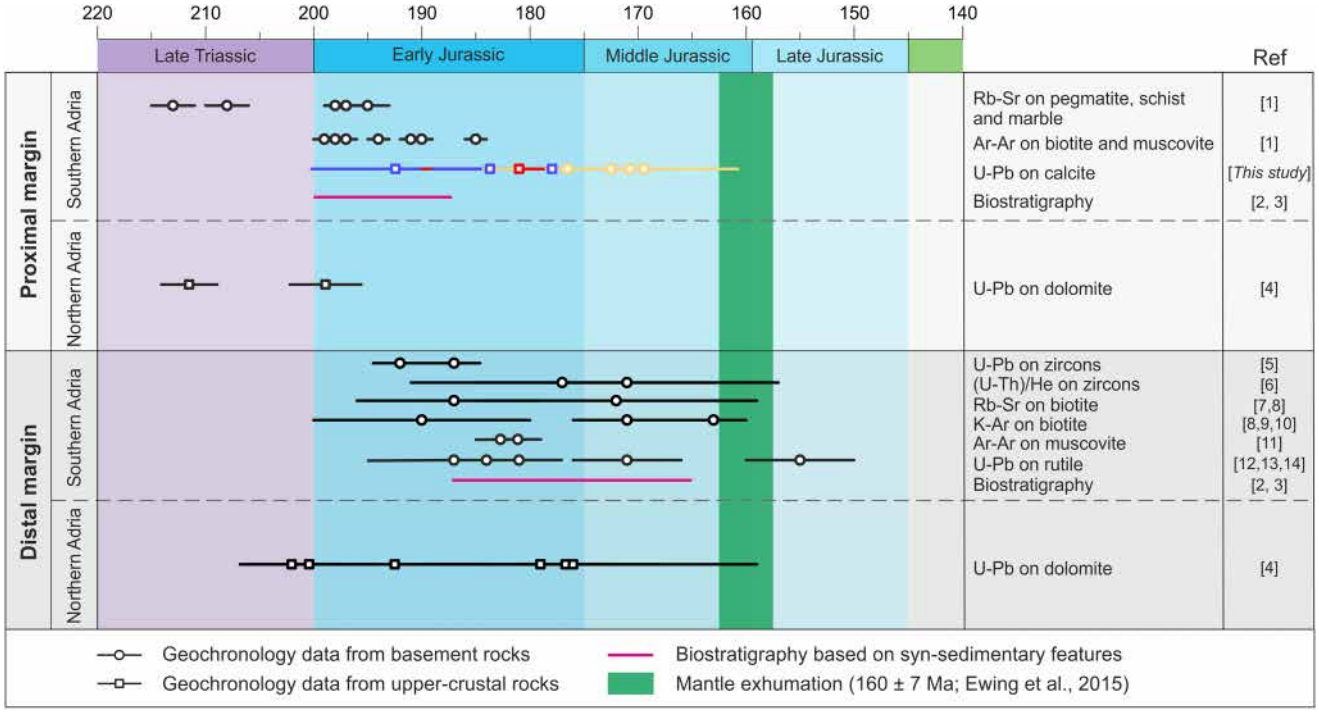

FIGURE 6 Summary of geochronological and biostratigraphic constraints for rift-related faults in the proximal and distal margin of southern and northern Adria. Radioisotopic ages from this study are reported with 2σ systematic error bars and colours corresponding to Figure 3a. [1] Bertotti et al. (1999); [2] Berra et al. (2009); [3] Santantonio and Carminati (2011); [4] Incerpi et al. (2020); [5] Galli et al. (2019); [6] Beltrando et al. (2015); [7] Jäger et al. (1967); [8] Hunziker (1974); [9] McDowell and Schmid (1968); [10] Wolff et al. (2012); [11] Mulch et al. (2002); [12] Zack et al. (2011); [13] Smye and Stockli (2014); and [14] Ewing et al. (2015). [Colour figure can be viewed at wileyonlinelibrary.com]

Norian—Rhaetian; Galli et al., 2007), even when 2σ uncertainties are considered. Individual Cal-1 U-Pb isochrones and corresponding ages are reported in Figures 5a,c, 6 and Supporting information S3.

5 | DISCUSSION

The new U-Pb radiometric ages presented herein (Figures 5a,c, 6 and Supporting information S3) provide the first absolute constraints on the onset of the Jurassic extensional regime in the Lombardian Basin, suggesting that the AF was active across the Early and Middle Jurassic.

Stratigraphic and sedimentological evidence indicate that the AF was active during the late Hettangian–Sinemurian, simultaneously with the deposition of Moltrasio Limestone (Figure 7a). Field-based observation of wedge-shaped deposits (Figure 7a) and slump folds statistical analysis (Figure 3d–f) in the hangingwall of the AF, along with palaeo-stress analysis of secondary AF-related faults in the footwall (Zu Limestone; Figure 3b,c) and hangingwall (Moltrasio Limestone; Figure 3e,g), all point out to a rift-related Early Jurassic activity of the AF.

Prior to this study, the timing of the Jurassic rift-associated faults was determined based on stratigraphic and sedimentological evidence in the Lower Jurassic units (Berra et al., 2009; Bertotti et al., 1993; Mattioli & Erba, 1999; Winterer & Bosellini, 1981). Geochronological constraints on the Early Jurassic rifting in the Adria proximal margin of Southern Alps are limited to intra-basement faults: ages from deformed Triassic pegmatites and mylonites in micaschists and marbles range from 215 ± 2 Ma to 185 ± 1 Ma (Bertotti et al., 1999) and partially overlap with the carbonate U-Pb dataset obtained here (Figure 4). U-Pb geochronology data obtained by Incerpi et al. (2020), related to the extensional activity recorded north of the Periadriatic Fault, in the proximal margin of northern Adria, also partially overlap (Figure 6).

All the pre-existing models suggested a Sinemurian age for rifting in the proximal margin, ceasing of tectonic activity at the end of Pliensbachian and shifting towards the Western Southern Alps from the Toarcian (Beltrando et al., 2015; Berra et al., 2009; Berra & Carminati, 2009; Manatschal et al., 2022; Santantonio & Carminati, 2011). In the hangingwall of the AF, the Toarcian–Bathonian succession (Concesio Group; Figure 7a) is more than 100 m thick, but totally missing on the Mt. Poieto–Nese high, while it is replaced by the Sogno Formation to the west (Figures 1b and 7a; Bertotti et al., 1993; Mattioli & Erba, 1999). The AF was hence active during the Middle Jurassic representing the bordering fault of the N-S trending Mt. Poieto–Nese high. In Mt. Rena half-graben, tilted-normal faults and slump folds are crosscut by later normal fault sets, consistent with the same extensional event (Figure 3e,g). U-Pb radiometric ages of this study, spanning from Hettangian to Callovian times (ca. 40 Ma considering 2σ systematic uncertainties; Figure 5a), support a long-lived extensional activity. This is further supported by decompacted subsidence curves calculated for Mt. Poieto–Nese high and Mt. Rena half-graben (Figure 5b), showing that the age of

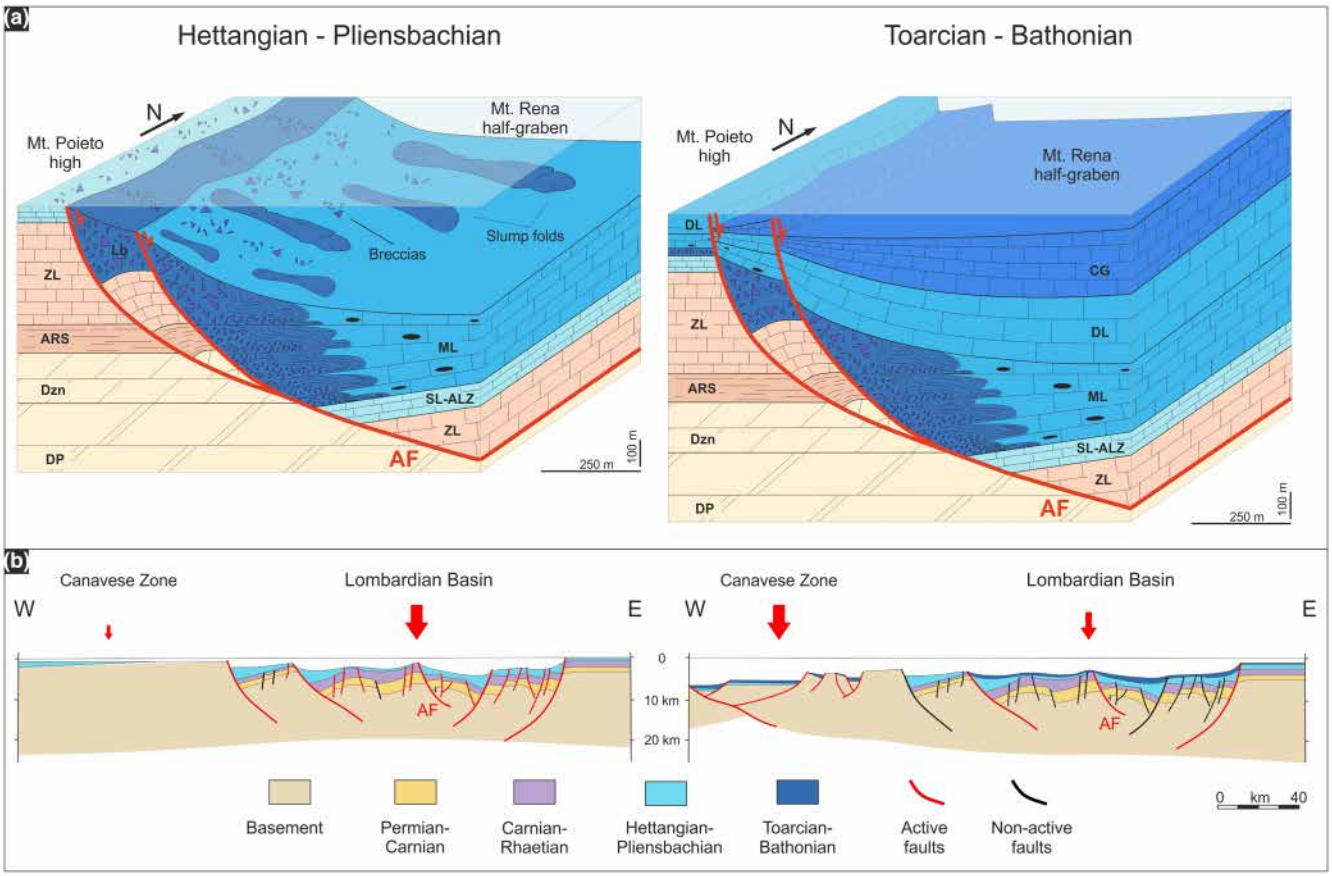

FIGURE 7 (a) Model of the fault-controlled Mt. Rena half-graben during the Hettangian–Pliensbachian and Toarcian–Bathonian. DP—Dolomia Principale; Dzn—Dolomie zonate; ARS—Riva di Solto Shales; ZL—Zu Limestone; SL-ALZ—Sedrina Limestone and Albenza Formation; Lb—Lower breccias of ML; ML—Moltrasio Limestone; DL—Domaro Limestone; CG—Concesio Group; and AF—Amora Fault. (b) Cartoon of the Lombardian Basin and Canavese Zone during Hettangian–Pliensbachian and Toarcian–Bathonian, respectively. The red arrows indicate rift-related activity, with intensity directly proportional to their size (modified from Santantonio & Carminati, 2011). [Colour figure can be viewed at wileyonlinelibrary.com]

differentiation between the footwall and the hangingwall of the AF fits well with U-Pb ages (Figure 5a,b).

As the precipitation of Cal-1 slickenfibres (180.9 ± 4.5|8.9 Ma) is considered synchronous with movement along the slip plane (Roberts & Holdsworth, 2022), this calcite represents the most reliable marker of syn-kinematic fault activity. However, blocky calcite in tension gashes can still be considered a reliable marker in dating syn-kinematic activity, since the duration between fracturing and calcite precipitation is typically shorter than the uncertainties associated with U-Pb dating, as suggested by Wei et al. (2023).

Recrystallization of Cal-1 crystals is not suggested by their uniform luminescence response (Figure 4b,c) and $\delta^{13}C_{carb}$ signature (Figure S2_b). Similarities in both luminescence and isotopic signature between Cal-1 and the host-rock (Figures 4 and S2_a) point to a closed hydrogeological system, where the calcite parent fluids were possibly buffered by the host rock, and this corroborates U-Pb results showing a typical closed system behaviour (Bilau et al., 2023).

According to this study, the onset of AF activity likely started around the end of the Hettangian, that is, ca. 3 Ma after the host rock deposition, consistent with the beginning of rift activity in the Lombardian Basin (Berra & Carminati, 2009; Berra et al., 2009; Santantonio & Carminati, 2011; Figures 6 and 7b) and in the Austroalpine proximal northern Adria margin (Incerpi et al., 2020; Figure 6).When rifting shifted westward around Toarcian times (Figures 6 and 7b; Berra & Carminati, 2009; Berra et al., 2009; Santantonio & Carminati, 2011; Beltrando et al., 2015; Manatschal et al., 2022), tectonic activity in the Lombardian Basin decreased, continuing with several pulses at least until Bathonian times, when mantle exhumation occurred in the Canavese zone (165 ± 7 Ma; Ewing et al., 2015; Figure 6). Field-based evidence and U-Pb ages show that the AF activity is partially coeval with rifting in the distal Adria margin (Figures 6 and 7b). Long-lived faults in extensional settings are common. An example is the Early Cenozoic rifting stage of the South China Sea proximal margin (Ye et al., 2018). This event is characterized by syn-rift low-angle normal faults bordering half-graben basins, recording two different tectonic stages (Hao et al., 2021): (i) formation of wedge-shaped half-graben strictly bounded by faults and (ii) later sedimentation slightly controlled by faults. A similar evolution can be also inferred in the study area: (i) deposition of the upper Hettangian–Pliensbachian succession, during the main activity of the AF (Figure 7a) and (ii) deposition of the Toarcian–Kimmeridgian succession, whose thickness is still controlled by the AF (Figure 7a).

6 | CONCLUSIONS

This study highlights the high potential of an integrated approach, based on multiscale structural and stratigraphic analyses combined with in-situ U-Pb dating of syn-tectonic calcite veins and slickenfibres, in shedding new light on fault activity at shallow crustal levels.

The integrated multidisciplinary approach used in this study allowed the reconstruction of:

(i) the geometrical features and kinematics of one of the main Early Jurassic extensional growth faults in the central Southern Alps and
(ii) the duration of fault activity, constrained by U-Pb ages that span from Hettangian to Callovian.

The proposed chrono-structural model implies a multi-stage evolution of the Amora Fault system. In the first stage, the Amora Fault bordered a strongly subsiding half-graben characterized by high sedimentation rates. Later, extension decreased though it still controlled syn-tectonic sedimentation. The activity of the AF better defines the evolution of the Southern Alps, where the extensional tectonics shifted from the Lombardian Basin to the distal margin of southern Adria since the Late Pliensbachian–Toarcian. Therefore, as documented by the data collected along the AF, the extension persisted in the Lombardian Basin, being synchronous with activity in the distal margin of Adria.

ACKNOWLEDGEMENTS

In-situ U-Pb analyses were performed at CEREGE with instruments acquired with support of the Initiative d'Excellence of Aix-Marseille University—A*Midex, DatCarb project. We thank G. Della Porta (University of Milan) and E. Ferrari (University of Milan) for their fundamental support during O-C stable isotope analysis. L. Angiolini (University of Milan) is warmly thanked for support in stratigraphic logging. N. Beaudoin and an anonymous reviewer are thanked for their insightful suggestions that greatly improve the paper. We also wish to thank C. Doglioni for editorial handling. This research has been financially supported by the Ministero dell'Università e della Ricerca (grant no. 2021-NAZ-0299, CUP: J33C22000170001).

CONFLICT OF INTEREST STATEMENT

There is no conflict of interest.

DATA AVAILABILITY STATEMENT

The data that supports the findings of this study are available in the supplementary material of this article.

ORCID

M. Rocca https://orcid.org/0000-0002-6493-6073
S. Zanchetta https://orcid.org/0000-0001-7690-969X

REFERENCES

Alsop, G. I., & Marco, S. (2012). A large-scale radial pattern of seismogenic slumping towards the Dead Sea Basin. *Journal of the Geological Society*, *169*, 99–110. https://doi.org/10.1144/0016-76492011-032

Beltrando, M., Stockli, D. F., Decarlis, A., & Manatschal, G. (2015). A crustal-scale view at rift localization along the fossil Adriatic margin of the Alpine Tethys preserved in NW Italy. *Tectonics*, *34*, 1927–1951. https://doi.org/10.1002/2015TC003973

Bernoulli, D. (1964). Zur Geologie des Monte Generoso. *Beiträge zur Geologischen Karte der Schweiz: Neue Folge*, *118*, 1–134.

Berra, F., & Carminati, E. (2009). Subsidence history from a backstripping analysis of the Permo-Mesozoic succession of the Central Southern Alps (Northern Italy): Subsidence history from backstripping analysis. *Basin Research*, *22*, 952–975. https://doi.org/10.1111/j.1365-2117.2009.00453.x

Berra, F., Galli, M. T., Reghellin, F., Torricelli, S., & Fantoni, R. (2009). Stratigraphic evolution of the Triassic-Jurassic succession in the Western Southern Alps (Italy): The record of the two-stage rifting on the distal passive margin of Adria. *Basin Research*, *21*, 335–353. https://doi.org/10.1111/j.1365-2117.2008.00384.x

Bersezio, R., Jadoul, F., & Chinaglia, N. (1997). Geological map of the Norian-Jurassic succession of the Southern Alps of Bergamo. An Explenatory Note. *Italian Journal of Geosciences*, *116*, 363–378.

Bertotti, G., Picotti, V., Bernoulli, D., & Castellarin, A. (1993). From rifting to drifting: Tectonic evolution of the South-Alpine upper crust from the Triassic to the early cretaceous. *Sedimentary Geology*, *86*, 53–76. https://doi.org/10.1016/0037-0738(93)90133-P

Bertotti, G., Seward, D., Wijbrans, J., Ter Voorde, M., & Hurford, A. J. (1999). Crustal thermal regime prior to, during, and after rifting: A geochronological and modeling study of the Mesozoic South Alpine rifted margin. *Tectonics*, *18*, 185–200. https://doi.org/10.1029/1998TC900028

Bilau, A., Bienveignant, D., Rolland, Y., Schwartz, S., Godeau, N., Guihou, A., Deschamps, P., Mangenot, X., Brigaud, B., Boschetti, L., & Dumont, T. (2023). The tertiary structuration of the Western Subalpine foreland deciphered by calcite-filled faults and veins. *Earth-Science Reviews*, *236*, 104270. https://doi.org/10.1016/j.earscirev.2022.104270

Casati, P., & Gaetani, M. (1968). Lacune nel Triassico Superiore e nel Giurassico del Canto Alto—Monte di Nese (Prealpi Bergamasche). *Bollettino della Societa Geologica Italiana*, *87*, 719–731.

Chenin, P., Manatschal, G., Ghienne, J., & Chao, P. (2022). The syn-rift tectono-stratigraphic record of rifted margins (part II): A new model to break through the proximal/distal interpretation frontier. *Basin Research*, *34*, 489–532. https://doi.org/10.1111/bre.12628

Delvaux, D., & Sperner, B. (2003). New aspects of tectonic stress inversion with reference to the TENSOR program. *Geological Society, London, Special Publications*, *212*, 75–100. https://doi.org/10.1144/GSL.SP.2003.212.01.06

Erba, E., Cavalheiro, L., Dickson, A. J., Faucher, G., Gambacorta, G., Jenkyns, H. C., & Wagner, T. (2022). Carbon- and oxygen-isotope signature of the Toarcian oceanic anoxic event: Insights from two Tethyan pelagic sequences (Gajum and Sogno cores—Lombardy Basin, northern Italy). *Newsletters on Stratigraphy*, *55*, 451–477. https://doi.org/10.1127/nos/2022/0690

Ewing, T. A., Rubatto, D., Beltrando, M., & Hermann, J. (2015). Constraints on the thermal evolution of the Adriatic margin during Jurassic continental break-up: U–Pb dating of rutile from the Ivrea–Verbano zone, Italy. *Contributions to Mineralogy and Petrology*, *169*, 44. https://doi.org/10.1007/s00410-015-1135-6

Frizon De Lamotte, D., Fourdan, B., Leleu, S., Leparmentier, F., & De Clarens, P. (2015). Style of rifting and the stages of Pangea breakup: Style of rifting and Pangea break-up. *Tectonics*, *34*, 1009–1029. https://doi.org/10.1002/2014TC003760

Gaetani, M. (1975). Jurassic stratigraphy of the Southern Alps: A review. *Geology of Italy*, *1*, 377–402.

Galli, A., Grassi, D., Sartori, G., Gianola, O., Burg, J.-P., & Schmidt, M. W. (2019). Jurassic carbonatite and alkaline magmatism in the Ivrea zone (European Alps) related to the breakup of Pangea. *Geology*, *47*, 199–202. https://doi.org/10.1130/G45678.1

Galli, M. T., Jadoul, F., Bernasconi, S. M., Cirilli, S., & Weissert, H. (2007). Stratigraphy and palaeoenvironmental analysis of the Triassic-Jurassic transition in the western Southern Alps (Northern Italy): Palaeogeography. *Palaeoclimatology, Palaeoecology*, *244*, 52–70. https://doi.org/10.1016/j.palaeo.2006.06.023

Hao, S., Mei, L., Shi, H., Paton, D., Mortimer, E., Du, J., Deng, P., & Xu, X. (2021). Rift migration and transition during multiphase rifting: Insights from the proximal domain, northern South China Sea rifted margin. *Marine and Petroleum Geology*, *123*, 104729. https://doi.org/10.1016/j.marpetgeo.2020.104729

Hunziker, J. C. (1974). Rb-Sr and K-Ar age determination and the Alpine tectonic history of the Western Alps. Mem. Ist. Geol. Miner. Univ. Padova, 31 p.

Incerpi, N., Martire, L., Manatschal, G., Bernasconi, S. M., Gerdes, A., Czuppon, G., Palcsu, L., Karner, G. D., Johnson, C. A., & Figueredo, P. H. (2020). Hydrothermal fluid flow associated to the extensional evolution of the Adriatic rifted margin: Insights from the pre- to post-rift sedimentary sequence (SE Switzerland, N ITALY). *Basin Research*, *32*, 91–115. https://doi.org/10.1111/bre.12370

Jadoul, F., & Galli, M. T. (2008). The Hettangian shallow water carbonates after the Triassic/Jurassic biocalcification crisis: The Albenza formation in the Western Southern Alps. *Rivista Italiana di Paleontologia e Stratigrafia*, *114*(3), 453–470. https://doi.org/10.13130/2039-4942/5911

Jäger, E., Niggli, E., & Wenk, E. (1967). Rb-Sr-Altersbestimmungen an Glimmern der Zentralalpen. *Beiträge zur Geologischen Karte der Schweiz, NF*, *134*, *67*.

Manatschal, G., & Bernoulli, D. (1998). Rifting and early evolution of ancient ocean basins: The record of the Mesozoic Tethys and of the Galicia-Newfoundland margins. *Marine Geophysical Research*, *20*, 371–381.

Manatschal, G., Chenin, P., Ghienne, J., Ribes, C., & Masini, E. (2022). The syn-rift tectono-stratigraphic record of rifted margins (part I): Insights from the Alpine Tethys. *Basin Research*, *34*, 457–488. https://doi.org/10.1111/bre.12627

Mattioli, E., & Erba, E. (1999). Synthesis of calcareous nannofossil events in tethyan lower and middle Jurassic successions. *Rivista Italiana di Paleontologia e Stratigrafia*, *105*, 343–376.

McDowell, F. W., & Schmid, R. (1968). Potassium-argon ages from the Valle d'Ossola section of the Ivrea-Verbano zone (northern Italy). *Schweizerische Mineralogische und Petrographische*, *48*, 205–210.

Mulch, A., Rosenau, M., Dörr, W., & Handy, M. R. (2002). The age and structure of dikes along the tectonic contact of the Ivrea-Verbano and Strona-Ceneri zones (Southern Alps, Northern Italy, Switzerland). *Schweizerische Mineralogische und Petrographische*, *82*, 55–76.

Naves De Lima Rodrigues, M. C., Trzaskos, B., Alsop, G. I., Farias Vesely, F., Mottin, T. E., & Buzatto Schemiko, D. C. (2021). Statistical analysis of structures commonly used to determine palaeoslopes from within mass transport deposits. *Journal of Structural Geology*, *151*, 104421. https://doi.org/10.1016/j.jsg.2021.104421

Nuriel, P., Craddock, J., Kylander-Clark, A. R. C., Uysal, I. T., Karabacak, V., Dirik, R. K., Hacker, B. R., & Weinberger, R. (2019). Reactivation history of the north Anatolian fault zone based on calcite age-strain analyses. *Geology*, *47*, 465–469. https://doi.org/10.1130/G45727.1

Nuriel, P., Weinberger, R., Kylander-Clark, A. R. C., Hacker, B. R., & Craddock, J. P. (2017). The onset of the Dead Sea transform based on calcite age-strain analyses. *Geology*, *45*, 587–590. https://doi.org/10.1130/G38903.1

Roberts, N. M. W., & Holdsworth, R. E. (2022). Timescales of faulting through calcite geochronology: A review. *Journal of Structural Geology*, *158*, 104578. https://doi.org/10.1016/j.jsg.2022.104578

Roberts, N. M. W., & Walker, R. J. (2016). U–Pb geochronology of calcite-mineralized faults: Absolute timing of rift-related fault events on the northeast Atlantic margin. *Geology*, *44*, 531–534. https://doi.org/10.1130/G37868.1

Santantonio, M., & Carminati, E. (2011). Jurassic rifting evolution of the Apennines and Southern Alps (Italy): Parallels and differences. *Geological Society of America Bulletin*, *123*, 468–484. https://doi.org/10.1130/B30104.1

Schönborn, G. (1992). Alpine tectonics and kinematic models of the central Southern Alps. *Memorie Scienze Geologiche Padova*, *44*, 229–393.

Smye, A. J., & Stockli, D. F. (2014). Rutile U–Pb age depth profiling: A continuous record of lithospheric thermal evolution. *Earth and Planetary Science Letters*, *408*, 171–182. https://doi.org/10.1016/j.epsl.2014.10.013

Wei, D., Gao, Z., Zhang, L., Fan, T., Wang, J., Zhang, C., Zhu, D., Ju, J., & Luo, W. (2023). Application of blocky calcite vein LA-MC-ICP-MS U–Pb dating and geochemical analysis to the study of tectonic–fault–fluid evolutionary history of the Tabei Uplift, Tarim Basin. *Sedimentary Geology*, *453*, 106425. https://doi.org/10.1016/j.sedgeo.2023.106425

Winterer, E. L., & Bosellini, A. (1981). Subsidence and sedimentation on Jurassic passive continental margin, Southern Alps, Italy. *AAPG Bulletin*, *65*, 394–421. https://doi.org/10.1306/2F9197E2-16CE-11D7-8645000102C1865D

Wolff, R., Dunkl, I., Kiesselbach, G., Wemmer, K., & Siegesmund, S. (2012). Thermochronological constraints on the multiphase exhumation history of the Ivrea-Verbano zone of the Southern Alps. *Tectonophysics*, *579*, 104–117. https://doi.org/10.1016/j.tecto.2012.03.019

Woodcock, N. H. (1979). The use of slump structures as palaeoslope orientation estimators. *Sedimentology*, *26*, 83–99. https://doi.org/10.1111/j.1365-3091.1979.tb00339.x

Ye, Q., Mei, L., Shi, H., Shu, Y., Camanni, G., & Wu, J. (2018). A low-angle normal fault and basement structures within the Enping Sag, Pearl River Mouth Basin: Insights into late Mesozoic to early Cenozoic tectonic evolution of the South China Sea area. *Tectonophysics*, *731–732*, 1–16. https://doi.org/10.1016/j.tecto.2018.03.003

Zack, T., Stockli, D. F., Luvizotto, G. L., Barth, M. G., Belousova, E., Wolfe, M. R., & Hinton, R. W. (2011). In situ U–Pb rutile dating by LA-ICP-MS: 208Pb correction and prospects for geological applications. *Contributions to Mineralogy and Petrology*, *162*, 515–530. https://doi.org/10.1007/s00410-011-0609-4

Zanchetta, S., Malusà, M. G., & Zanchi, A. M. (2015). Precollisional development and Cenozoic evolution of the Southalpine retrobelt (European Alps). *Lithosphere*, *7*, L466.1. https://doi.org/10.1130/L466.1

SUPPORTING INFORMATION

Additional supporting information can be found online in the Supporting Information section at the end of this article.

Supplementary Information 1.

Supplementary Information 2.

Supplementary Information 3.

Table S1.

Table S3.

How to cite this article: Rocca, M., Zanchetta, S., Gasparrini, M., Mangenot, X., Berra, F., Deschamps, P., Guihou, A., & Zanchi, A. (2024). U-Pb carbonate dating reveals long-lived activity of proximal margin extensional faults during the Alpine Tethys rifting. *Terra Nova*, *36*, 347–357. https://doi.org/10.1111/ter.12717